High-Accuracy Corridor Mapping Without GCPs: Assessing Precisions of DSMs Generated from UAS Photogrammetry with On-Site Pre-Calibration

Kalima Pitombeira [1], Edson Mitishita [1], Charles Toth [2], Natália Amorim [1], Marcelo de Abreu [3]

[1] Geomatics Department, Federal University of Paraná, Curitiba, PR, Brazil – kalimapitombeira@ufpr.br, mitishita@ufpr.br, carvalho.natalia03@gmail.com
[2] Dept. of Civil, Environmental and Geodetic Engineering, The Ohio State University, Columbus, OH, USA – toth.2@osu.edu
[3] Tecsystem Company, Castelo, ES, Brazil – marcelo@imaginair.com.br

Keywords: Digital Elevation Model (DEM), *In-situ* camera calibration, On-the-job camera calibration, Unmanned Aerial Vehicle (UAV); GNSS-Assisted Aerial Triangulation.

Abstract
High-resolution Digital Surface Models (DSMs) are crucial for diverse geospatial analyses and UAS photogrammetry offers a cost-effective option for DSM acquisition. However, corridor mapping, due to its linear geometry, challenges the extraction of 3D information without relying on Ground Control Points (GCPs). While onboard GNSS-RTK can improve accuracy, robust camera calibration is critical to mitigate systematic vertical errors propagating in derived DSM. Existing research lacks sufficient investigation into feasible pre-calibration strategies for corridor mapping without GCPs. Therefore, this study addresses this gap by evaluating the precision of DSMs obtained from five photogrammetric experiments without GCPs: one on-the-job calibration and four GNSS-Assisted Aerial Triangulation using on-site pre-calibrations with different sub-blocks of images. For precision assessment of DSMs, a reference experiment with 17 GCPs and all available images was also carried out. Our results show that including oblique images in on-site pre-calibration with sub-blocks significantly reduced the critical correlation between focal length and Z object-space coordinates (from 99% to less than 20%). That outcome directly influenced focal length estimation and allowed mitigation of vertical bias in generated DSMs. The results demonstrate that on-site pre-calibration notably improved the accuracy and precision of vertical spatial data acquisition. These findings highlight on-site oblique pre-calibration with a sub-block of images as a feasible and robust strategy for producing high-resolution 3D models in UAS corridor mapping, significantly reducing reliance on GCPs.

1. Introduction

High-resolution Digital Surface Models (DSMs) provide detailed 3D information on Earth's surface features and are fundamental to various geosciences, engineering, and environmental analyses (Darji *et al*., 2024). DSMs are geospatial representations of the elevation from the ground surface and the elements above, including vegetation, buildings, transmission lines, vehicles, poles, and other man-made objects (Guth *et al*., 2021). Therefore, DSMs can be used in several applications, such as performing archaeological investigations (Şenkal *et al*., 2021), canopy height analyses (Hashimoto *et al*., 2025), and urban planning (Skondras *et al*, 2022). The quality and resolution of these 3D models directly impact the reliability of subsequent analyses. Therefore, before using DSMs as a reference elevation surface, it's crucial to ensure their accuracy meets the specific application's requirements. DSMs can be acquired through various methods, including terrestrial surveys (e.g., geodetic, topographic), remote sensing (e.g., LASER - Light Amplification by the Stimulated Emission of Radiation - scanning, radar, orbital, and aerial imagery), and global digital elevation models (e.g., ASTER, SRTM, GTOPO30) (Brock *et al*., 2020, Huang *et al*., 2022). Among those, remote sensing applications are widespread and cost-effective for obtaining high-resolution DSMs with high accuracy (Štroner *et al*., 2023).

In that context, Unmanned Aerial Systems (UAS), also known as Unmanned Aerial Vehicles (UAVs), have emerged as a popular platform for aerial surveys. They support both photogrammetric and laser scanning (LiDAR - Light Detection and Ranging) techniques due to their ease of use, automated flight configurations, remote-control capabilities, and the availability of consumer-grade sensors (Liu *et al*., 2022). However, the cost of LiDAR sensors may still pose a limiting factor for certain applications. Alternatively, UAS photogrammetry, utilizing the Structure from Motion – Multi-view Stereo (SfM-MVS) workflow, presents a lower-cost option, as laser sensors typically are more expensive than off-the-shelf cameras (Pinton *et al*., 2023). UAS photogrammetry with SfM-MVS enables high levels of automation for robust spatial data acquisition (Deliry and Avdan, 2021). Furthermore, SfM-MVS performs exceptionally well in generating dense point clouds and high-resolution DSMs (Pessoa *et al*., 2020), even considering varying conditions of light, scale, and image rotation (Smith *et al*., 2016)

One particularly challenging application of UAS photogrammetry lies in the spatial data acquisition of long linear features, such as rivers, pipelines, roads, and railways. Usually known as corridor mapping, the flight pattern required for this type of feature relies on long, mostly straight flight strips (commonly two strips in opposite directions). This results in an image block dimension where the length along the flight direction is significantly greater than the width (Andaru *et al.,*2022, Amorim and Mitishita, 2024). In that sense, estimating the roll orientation angle (around X axis) in the Bundle Adjustment tends to be more complicated, considering that corridor block geometry lacks observations in the cross-track direction (perpendicular to the corridor flight direction) which are crucial for accurately determining the images' roll angle. Some important applications of corridor mapping include road and railway planning (Ait-Lamallam *et al*, 2025), transmission pipeline geometric evaluation (Lenda *et al*., 2023), and river geomorphological studies (La Salandra et al., 2023).

Due to its geometric conditions, corridor mapping commonly requires a high degree of forward and side image overlap and dense deployment of well-distributed Ground Control Points (GCPs) to ensure high-accuracy 3D spatial data acquisition (Ferrer-González *et al*., 2020). On the other hand, using numerous GCPs requires extensive field surveys, which can be costly in areas with difficult access (e.g., dense vegetation, glacial regions, hilly terrain) or even offer risk to human health in hazard situations (e.g., floods, earthquakes, wildfires) (Chiabrando *et al*., 2019). Thus, it is crucial to explore solutions that can mitigate or eliminate the need for GCPs without compromising the accuracy of photogrammetric data extraction.

One method for reducing the required GCP usage in UAS photogrammetry is by acquiring camera station coordinates and orientation angles using onboard Global Navigation Satellite

This contribution has been peer-reviewed. The double-blind peer-review was conducted on the basis of the full paper.
https://doi.org/10.5194/isprs-annals-X-3-W4-2025-293-2026 | © Author(s) 2026. CC BY 4.0 License.

System (GNSS) receivers and Inertial Navigation Systems (INS) (Carbonneau and Dietrich, 2017). However, high-precision INS for UAS can be costly and/or not feasible to carry during flight due to payload limitations. Conversely, UAS equipped with high-accuracy GNSS receivers have become increasingly popular and less expensive, enabling camera coordinates to be computed by Real-Time Kinematic (RTK) or Post-Processed Kinematic (PPK) (Zhang *et al*., 2019). When only the camera position is available, a supported block orientation can be performed by fixing or constraining the camera station coordinates in the BA as additional observations. This approach is known as GNSS-Assisted Aerial Triangulation (GNSS-AAT) or GNSS-Assisted Integrated Sensor Orientation (Forlani *et al*., 2018).

It's important to note that while directly measured camera positions can reduce the need for GCPs, the accuracy of 3D information extraction without GCPs relies on precise camera calibration (Mitishita *et al.*, 2014). For example, slight inaccuracies in lens distortion parameters can reflect a radial systematic error in the dense point cloud and DSM surface generated, known as dome/bowl deformations (Wackrow and Chandler, 2008; Carbonneau and Dietrich, 2017). To obtain a robust camera calibration estimation, one might initially conclude that performing pre-calibration (i.e., prior to the spatial data acquisition) in a test field with a large number of GCPs with known object coordinates is a viable option. This would be particularly true when utilizing metric cameras for aircraft photogrammetry. However, low-cost non-metric UAS cameras exhibit less stability, and their internal elements are more sensitive to minor vibrations, temperature variations, and landing impacts, therefore, it is not common to assume that the IOPs remain unchanged between different surveys (Cledat *et al*., 2020). In contrast, on-the-job calibration consists of an on-site (*in situ*) calibration that simultaneously estimates the interior orientation and 3D object coordinates, using the same images obtained for the actual spatial data acquisition (Kraus, 2007). On-the-job is most frequently adopted for UAS photogrammetry since the IOPs are estimated with the same dataset and flight conditions (Sobura, 2021). Nevertheless, on-the-job calibration can result in local or non-real solutions when highly correlated parameters (e.g., focal length and the Z_s coordinate of the camera station) are estimated within the same adjustment (Sanz-Ablanedo *et al*., 2020), therefore, that calibration may not be accurate or reliable when using a weak block geometry, such as vertical images in flat terrain (Remondino and Fraser, 2006).

In this regard, camera calibration can be improved by reducing the correlation between parameters. This can be achieved through various strategies, such as employing different flight patterns (e.g., including cross-strips, multiple flight heights, and oblique imagery) and using direct measurements of camera positions and orientations as fixed and/or constrained on the BA (Luhmann *et al*., 2006; Remondino and Fraser, 2006). Another alternative is performing on-site (*in situ*) pre-calibration with sub-blocks of images, which means the calibration is performed prior to the spatial acquisition, i.e., IOPs are estimated in a different BA from 3D information extraction. However, the calibration is performed on-site with a subset of images obtained in the same survey, therefore in the same flight conditions. Promising results were achieved using on-site pre-calibration for improving the accuracy of spatial data acquisition both for aircraft (Costa *et al*. 2018) and UAS imagery (Pitombeira and Mitishita, 2023) though it required a minimum configuration of GCPs within the sub-block.

For corridor mapping, as previously discussed, the block geometry involves long flight strips, making it challenging to implement most flight pattern strategies that could reduce parameter correlation in on-the-job camera calibration since it is rarely feasible to conduct multiple flights along the entire corridor (Andaru *et al*., 2020). On the other hand, performing on-the-job calibration with only nadir images could lead to inaccuracies in IOPs due to high correlations between estimated parameters, negatively impacting the accuracy of spatial information extraction, dense point clouds, and DSMs of the corridor. Conversely, performing a pre-calibration in a test field could easily yield IOPs that do not properly model the flight conditions of UAS data acquisition, due to camera instabilities, and thus would also affect the resulting 3D information accuracy.

In this context, achieving high-accuracy corridor mapping using UAS photogrammetry without GCPs remains a challenge, partially due to the difficulty of performing a reliable camera calibration. Findings from related studies on corridor mapping, such as Meinen and Robinson (2020), Ferrer-González *et al*. (2020), Andaru *et al.,* (2022) and Pilartes-Congo *et al*. (2024) reinforce two key points: 1) When using indirect georeferencing, a dense configuration of GCPs is required to achieve high-accuracy spatial data acquisition; 2) When well-distributed GCPs are unavailable, using camera positions measured by an on-board GNSS receiver can improve spatial data acquisition, though it is insufficient to eliminate vertical bias and ensure high altimetric accuracy.

In previous work (Pitombeira *et al*., 2025) it was shown that performing on-site (*in situ*) pre-calibration with sub-blocks of vertical and oblique images, obtained at multiple flight heights, provides a more feasible method for incorporating multiple flight patterns and oblique images in corridor mapping. The outcomes revealed that the vertical accuracy of tie-point extraction on a road corridor was significantly improved in GNSS-AAT experiments, which constrained camera station coordinates obtained by GNSS-RTK and operated without GCPs. Despite these promising results, the study was restricted to evaluating the influence of on-site pre-calibration with sub-blocks of multi-height vertical and oblique images solely for the estimation of tie-point 3D coordinates on the corridor site. To our knowledge, there is a lack of studies evaluating the impacts of on-site pre-calibration with image sub-blocks on subsequent 3D products of photogrammetric processing from corridors, such as dense point clouds and DSMs. These analyses are of great importance when considering a wide range of photogrammetric applications that require high-level feature extractions based on digital models, as previously discussed (e.g., road planning and coastal monitoring).

Therefore, as a continuation of ongoing research, it is important to evaluate if this workflow is also robust for mitigating systematic errors (derived from IOP inaccuracies) in UAS-based DSMs of corridors. To address this gap, the present study aims to evaluate the precision of DSMs generated from: one experiment of on-the-job camera calibration with vertical images and four experiments of GNSS-AAT utilizing on-site camera pre-calibration with various configurations of sub-blocks including oblique images A reference experiment, performing on-the-job calibration with indirect georeferencing (using 17 targets as GCPs), was conducted to generate a DSM reference surface. The precision of these DSMs will be assessed by performing a Difference of DSM (DoD) against the reference surfaces and analyzing statistical metrics such as the median and Interquartile range (IQR).

2. Methodology

All the coordinates used in this work are referred to the horizontal Datum Geodetic Reference System for the Americas 2000 (SIRGAS 2000) and projected on Universal Transverse Mercator (UTM) Zone 24 South. The elevation values, representing orthometric heights, were referred to the vertical Datum of Imbituba, Santa Catarina, Brazil.

2.1 Study Site

The study site consists of a corridor of 3.2 km × 450 m around a state road (ES-166) located on Cachoeiro de Itapemirim city, Espírito Santo, in southeastern Brazil, as shown in Figure 1. This corridor covers an area of nearly 138 ha and is located on a hilly terrain in a countryside non-urbanized area, with elevations varying up to 110 m (70 to 180 m above mean sea level) and center coordinates of 20°41'23"S and 41°12'12"W (SIRGAS2000).

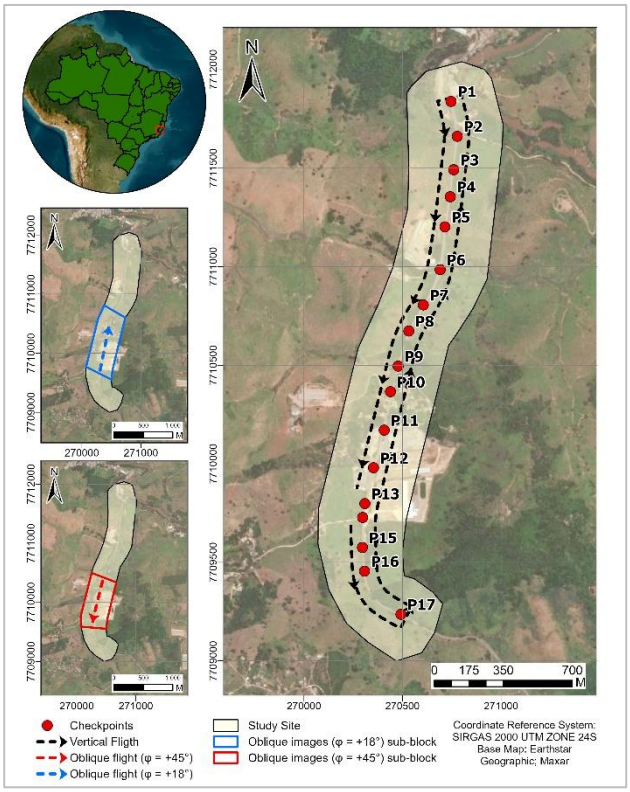

Figure 1. Study site and flight configurations.

2.2 Survey Specifications

Previous to the aerial survey, 17 signalized targets were distributed along both sides of the road for accuracy assessment, to be used as checkpoints. All targets were positioned solely on the road surface. This was due to the difficult access posed by the surrounding hilly topography and dense vegetation. This distribution, while serving to support Z-coordinate assessment, limits observations for horizontal (X and Y) accuracy determination. The geodetic field survey for determinate checkpoints' 3D coordinates was performed with two Topcon GNSS RTK receivers (base station and rover), model Hiper SR, with nominal horizontal precision of 10 mm + 0.8 ppm and vertical of 15 mm + 1.0 ppm.

DJI Matrice 350 RTK, a vertical take-off and landing multi-rotor UAS, was employed for the aerial survey. According to the manufacturer, its on-board GNSS RTK receiver, used for directly measuring camera positions, supports observations from GPS, GLONASS, BeiDou, and Galileo constellations. This system boasts a nominal precision of 1 cm+1 ppm horizontally and 1.5 cm+1 ppm vertically. For image acquisition, the DJI Zenmuse P1 camera, equipped with a global mechanical shutter, was utilized. This camera features a pixel size of 4.39 µm, a nominal focal length of 35 mm, a full-frame sensor measuring 35.9 mm x 24 mm, and 45 MP (image size of 8192 x 5460 pixels).

Three aerial flight configurations were employed in this work. The first and main survey involved the acquisition of a corridor block with 279 nadir images across two parallel strips, flown at 320 m flight height above ground level (AGL), with an 80% forward and 60% side overlap, resulting in a 3.8 cm/pixel average Ground Sample Distance (GSD). Two separate oblique image sub-blocks were obtained at a lower altitude of 200 m flight height AGL. One sub-block included 19 images at an 18° pitch (φ =+18°), covering a 1.5 ha area over 870 m of the road. The second sub-block included 21 images at a 45° pitch (ϕ=+45°), covering 2.7 ha over the same 870 m linear extent.

2.3 Data Processing Specifications

Agisoft Metashape Professional version 2.1.2 was used to perform all photogrammetric data processing with Structure from Motion – Multi-View Stereo (SfM-MVS) workflow. For automatic tie point extraction and matching, images were upscaled by a factor of 4 (*Highest* setting), and a maximum threshold of 40,000 feature points and 4,000 tie points per image was established. For the BA, the precision of tie points image coordinates was set as 1 pix (4.39 µm).

Brown's distortion model was used to compute sensor interior orientation for all camera calibrations performed in this study. The estimated parameters included focal length (c), principal point coordinates (x_P, y_P), radial symmetric distortion coefficients (k_1, k_2, k_3), and decentering distortion coefficients (p_1, p_2).

Dense point clouds were generated, in Metashape photogrammetric experiments, using depth maps as the source data. This process utilizes the camera's exterior and interior orientation parameters, estimated previously by the BA, to compute depth maps from overlapping image pairs. Metashape's *Point Cloud Confidence* feature was used to quantify the number of contributing depth maps for every point in the dense point cloud, which indicates the robustness of the point's geometric estimation. To manage the high computational demands of this step, images were downscaled by a factor of 16 (four times per side) using the software's *Medium* setting. To enhance point cloud resolution and retain feature details, the outlier filter mode was configured as *Mild*, however, this setting could increase the data's susceptibility to outliers.

Before generating Digital Surface Models (DSMs) from the dense point cloud, a pre-filtering step was employed to improve precision. For our corridor dataset, point confidence values ranged from 1 to 255 depth maps, representing the number of combined depth maps used to estimate each point's position. Preliminary investigations revealed that points generated from a maximum of 3 depth maps were predominantly situated at the outer boundaries of the block or along the edges of features such as buildings and vegetation. Therefore, removing these points (derived from 3 or fewer depth maps) allowed to improve point cloud confidence without significantly compromising the overall density, while also ensuring more reliable outer boundaries for subsequent DSM generation.

After the confidence filter, the point cloud served as source data for Digital Surface Model (DSM) generation. For this process, all points were utilized, i.e., both bare earth and features above the ground were included. DSM generation was performed using interpolation, which allows for filling holes, caused by areas without points, in the final model surface

This contribution has been peer-reviewed. The double-blind peer-review was conducted on the basis of the full paper.
https://doi.org/10.5194/isprs-annals-X-3-W4-2025-293-2026 | © Author(s) 2026. CC BY 4.0 License.

	Calibration parameters	Sub-block of images used for on-site pre-calibration	Images used for spatial data acquisition
OTJCalib	Estimated IOPs	-	279 (Vertical, 320 m)
GNSS_AAT_1	Fixed IOPs from OSCalib_1	OSCalib_1: 40 (Vert, 320 m)	279 (Vertical, 320 m)
GNSS_AAT_2	Fixed IOPs from OSCalib_2	OSCalib_2: 40 (Vert, 320 m), 19 (Obliq 18°, 200 m)	279 (Vert, 320 m), 19 (Obliq 18°, 200 m)
GNSS_AAT_3	Fixed IOPs from OSCalib_3	OSCalib_3: 40 (Vert, 320 m), 21 (Obliq 45°, 200 m)	279 (Vert, 320 m), 21 (Obliq 45°, 200 m)
GNSS_AAT_4	Fixed IOPs from OSCalib_4	OSCalib_4: 40 (Vert, 320 m), 19 (Obliq 18°, 200 m), 21 (Oblique +45°, 200 m)	279 (Vert, 320 m), 19 (Obliq 18°, 200 m), 21 (Obliq +45°, 200 m)

Table 1. Details of photogrammetric experiments.

Therefore, to meet the goal of evaluating the influence of on-site camera pre-calibration on the precision of DSMs in corridors without GCPs, this study performed five experiments of camera calibration:

- One on-the-job calibration (OTJCalib) using the corridor block with 279 vertical images acquired at 320 m flight height AGL;
- Four on-site pre-calibrations with different configurations of sub-blocks (OSCalib_1 to OSCalib_4), including vertical (320 m flight height AGL) and oblique (200 m flight height AGL) images.

Subsequently, four GNSS-Assisted Aerial Triangulation (GNSS-AAT) experiments (GNSS-AAT_1 to GNSS-AAT_4) were performed. Each of these used a specific set of IOPs estimated from one of the on-site camera pre-calibrations. To fully assess the impact of these configurations, the same sub-block of oblique images used in the corresponding on-site pre-calibration was also included in the GNSS-AAT experiments. This approach enabled the analyses of how each oblique sub-block configuration influenced the entire photogrammetric process, from the calibration step through to 3D geo-information extraction (tie points, dense point cloud, and DSM). Details of all experiments performed on Metashape can be found in Table 1.

Given Metashape's restrictions on accessing essential Bundle Adjustment data, particularly parameter correlations, the Federal University of Paraná's (UFPR) Calibration Bundle Adjustment (CALIBRA) was employed. CALIBRA software, which uses a traditional photogrammetry workflow, enabled more comprehensive investigations into parameter correlations. Thus, the four on-site pre-calibration experiments using image sub-blocks (OSCalib_1 to OSCalib_4) were replicated on CALIBRA. For these, sub-samples of automatically extracted tie points (up to 1200 points) from Metashape were used. The precision for tie points' image coordinates was set at 1 pixel.

Across all photogrammetric experiments (Metashape and CALIBRA), the camera station coordinates (X_s, Y_s, Z_s) directly measured by the on-board GNSS-RTK were constrained by the RTK precision for each image (average RMSE of X_s: 0.012 m; Y_s: 0.013 m; Z_s: 0.037 m) and used as additional observations on the BA. Given the low accuracy of the onboard INS, camera orientation angles (ω, φ, κ) were only used as initial values and set as unknown to be estimated by the BA.Accuracy and Precision Assessment
The accuracy of the five spatial data acquisition experiments (OTJCalib and GNSS-ATT_1 to GNSS-ATT_4) was assessed using the Root Mean Square Error (RMSE) of 17 checkpoint discrepancies. These discrepancies represent the difference between the 3D coordinates of checkpoints obtained through the photogrammetric intersection and their field-surveyed coordinates (ground truth).

For an accurate assessment of the photogrammetrically generated DSMs, LiDAR-based DSMs offer comparable high-resolution and superior accuracy, making them commonly used as ground truth surfaces. However, due to the elevated costs of LiDAR sensors, LiDAR-based DSMs weren't available for the study site. Therefore, in this study, the accuracy of the photogrammetric-based DSM couldn't be directly evaluated. Alternatively, the DSMs' precision could be assessed. DSMs generated by on-the-job calibration or GNSS-AAT without GCPs can be compared to a reference experiment (REF_Calib) with a robust GCP distribution. For that purpose, we assumed the best possible photogrammetric experiment (REF_Calib) would involve an on-the-job calibration using: all 17 targets available as GCP, a block configuration including all images available (the vertical block and two oblique sub-blocks), and the camera station coordinates (X_s, Y_s, Z_s) directly measured by the on-board GNSS-RTK constrained by the RTK survey precision. All previously described steps for tie-point extraction, dense point cloud, and DSM generation were followed for this reference experiment.

Then, the Difference of DSM (DoD) was performed by subtracting the elevation values of the estimated DSMs (OTJCalib and GNSS-ATT_1 to GNSS-ATT_4) from the Reference DSM (Ref_Calib). This DoD operation was executed at a pixel level using the raster calculator within QGIS software version 3.14.11 via Python API. Consequently, the pixel values from the DoD could represent the elevation residuals of the estimated DSMs.

First, qualitative analyses of DoD outcomes were carried out to investigate the existence of spatially distributed bias. Afterward, the elevation residuals were used to compute statistic metrics for quantitative analyses of the estimated DSMs' precision. Noises on the generated DSMs led to high-magnitude outliers (up to 30 m). While initial analyses included RMSE of the elevation residuals, this metric is known to be less robust to outliers. Therefore, to ensure the robustness of the comparative analyses, the precision analysis on elevation residuals was performed with the Median and Interquartile range (IQR), as these are more outlier-robust metrics, in which IQR is given by the range between the data's 3rd and 1st quartiles.

3. Results and Discussion

3.1 Camera Calibration

Firstly, the IOPs estimated from the five camera calibrations (OTJCalib and OSCalib_1 to OSCalib_4) performed without GCPs were analyzed. Those experiments showed no significant variations among their values of principal point coordinates and lens distortion parameters. For focal length, the estimated values in the five calibrations were: 35.990 mm for OTJCalib, 35.977 mm for OSCalib_1, 35.972 mm for OSCalib_2, and 35.970 mm

for both OSCalib_3 and OSCalib_4. Therefore, it is notable that the focal length from OTJCalib has significant discrepancies when compared to on-site pre-calibrations, with up to 0.020 mm (4.6 pix) between OTJCalib and OSCalib_3/OSCalib_4. When comparing only the four on-site camera pre-calibrations, focal length values still have variations, however with a maximum discrepancy of 0.007 mm (1.6 pix) between OSCalib_1 and OSCalib_3/OSCalib_4. More details of camera calibration results (parameters and precisions) can be found at Pitombeira *et al*., 2025.

To our current understanding, Metashape only allows access to the correlation matrix between estimated IOPs, and it isn't possible to extract the correlation matrix between other parameters, not even by the Python API. Therefore, the four on-site pre-calibrations with image sub-blocks were reproduced on CALIBRA software. Figure 2 displays the correlation values computed from the variance-covariance matrix on experiments performed in CALIBRA software.

As shown in Figure 2, correlations of principal point coordinates (x_P, y_P) and focal length (c) between camera station coordinates (X_S, Y_S, Z_S) are very low, regardless of the on-site pre-calibration experiments. This outcome indicates that constraining direct camera positions allows those parameters to be refined during the Bundle Adjustment (BA) while still maintaining a low correlation with the estimated Interior Orientation Parameters (IOPs).

On the other hand, a high correlation (above 70%) appears between principal coordinates and pitch/roll orientation angles. Due to the low quality of the onboard INS, these orientation angles were set as unknown on the BA and, thus, calculated simultaneously with the IOPs. Normally, inaccuracies in principal point coordinate estimation can be associated with a high correlation between X_S/Y_S. However, as camera coordinates were constrained by the on-board RTK survey precision, these imprecisions became associated with the estimated orientation angles instead. It is important to note that these high correlations remained consistent across all calibrations. This indicates that adding a sub-block of oblique images wasn't sufficient to reduce correlations regarding the estimation of principal point coordinates. In such scenarios, the sub-block geometry could be improved by including cross-strips or incorporating rotations in the roll axis.

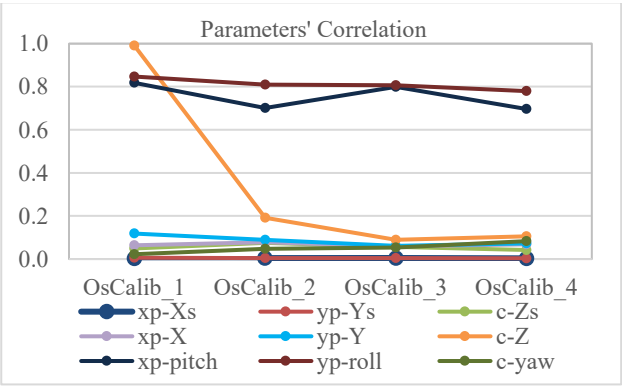

Figure 2. Parameters' correlations obtained in CALIBRA.

Another important finding can be found by analyzing focal length correlations. Despite showing no notable correlation with any EOPs, the focal length exhibited a significantly high- correlation of 99% with the Z coordinate of tie-points for the OSCalib_1, which used only vertical images. This outcome suggests that focal length and Z coordinates are almost entirely linear dependent in the BA, likely due to a lack of scale information in the vertical direction along the Z axis (Luhmann *et al*., 2006), which was expected considering that narrow corridors are usually close to a flat surface.

As the Z_S camera coordinate was constrained and no GCP was used, this scale issue made it difficult to precisely determine the focal length. This can lead to local solutions and, consequently, systematic errors in the acquired 3D information. On the other hand, the correlation between focal length and Z object-space coordinate dramatically dropped to less than 20% when any sub-block of oblique images was added – whether at an 18° inclination (OSCalib_2), a 45° inclination (OSCalib_3), or both (OSCalib_4). Therefore, even a small set of oblique images could successfully improve scale information along the vertical direction and reduce focal length correlations when using on-site camera pre-calibrations with sub-blocks.

3.2 Accuracy Assessment of Spatial Data Acquisition

For accuracy assessment of the five experiments of spatial data acquisition (OTJCalib and GNSS-AAT_1 to GNSS-AAT_4), the Root Mean Square Error (RMSE) values for the 17 checkpoints' discrepancies were calculated for both the horizontal (XY) and vertical (Z) components. Horizontal RMSE outcomes revealed low variation in accuracy across the experiments, with values ranging from 0.061 m (1.6 GSD) in GNSS-AAT_4 to 0.093 m (2.4 GSD) in GNSS-AAT_1. These results are supported by the camera calibration results since parameters associated with horizontal accuracy (e.g., principal point coordinates) showed neither significant variations in their estimated values nor changes in their correlations with other parameters. In contrast, vertical accuracy results showed notable improvements when comparing spatial data acquisition by the on-the-job calibration experiment (with only vertical images) to the GNSS-AAT experiments that included sub-blocks of oblique images. The vertical RMSE calculated for the OTJCalib experiments was 0.154 m (4.0 GSD). In contrast, GNSS-AAT experiments demonstrated improvements ranging from 67% in GNSS-AAT_1 with RMSE Z of 0.051 m (1.3 GSD) to 79% in GNSS-AAT_2 with RMSE Z of 0.032 m (0.8 GSD).

Those outcomes are related to the camera calibration results: when oblique images were added, the correlation between focal length and Z-point coordinates decreased substantially, from 99% to less than 20%. Moreover, the estimated focal length value also changed significantly, showing discrepancies of up to 4.6 pix when comparing on-the-job calibration to on-site camera pre-calibrations. In this context, adding even a small set of oblique images for camera calibration consistently reduced the linear dependency between parameters in the BA, which led to a more accurate estimation of focal length value and, therefore, improvements in vertical accuracy of up to 79% in spatial data acquisition. More detailed discussions of the extracted 3D information accuracy in those experiments can be found at Pitombeira *et al*., 2025.

3.3 Precision Assessment of Digital Surface Models

Next, to allow the precision assessment of Digital Surface Models (DSMs), one reference photogrammetric experiment (Ref_Calib) was performed using 17 signalized GCPs and all available images (vertical block and two oblique sub-blocks). This aimed to generate one DSM reference surface (Ref_DSM). Subsequently, a Difference of DSM (DoD) was computed by calculating the elevation difference between each pixel of the estimated DSMs (generated in the five spatial data acquisition experiments) and the reference DSM. Therefore, five DoD surfaces were computed for DSMs precision evaluation, in which: Figure 3a for OTJCalib, Figure 3b to GNSS-AAT_1, Figure 3c to GNSS-AAT_2, Figure 3d to GNSS-AAT_3 and Figure 3e to GNSS-AAT_1.

This contribution has been peer-reviewed. The double-blind peer-review was conducted on the basis of the full paper.
https://doi.org/10.5194/isprs-annals-X-3-W4-2025-293-2026 | © Author(s) 2026. CC BY 4.0 License.

Analyzing the residual results, it is notable that the DoD between OTJCalib_DSM and Ref_DSM (Figure 3a) shows a negative bias across the entire corridor, with higher discrepancies in the south area highlighted by dark red. Comparing the DoD between GNSS-AAT_1_DSM and Ref_DSM (Figure 3b), a notable negative bias still persists across most of the corridor, however, with lower elevation residuals (light red) and some positive residuals on the northern area (light blue).

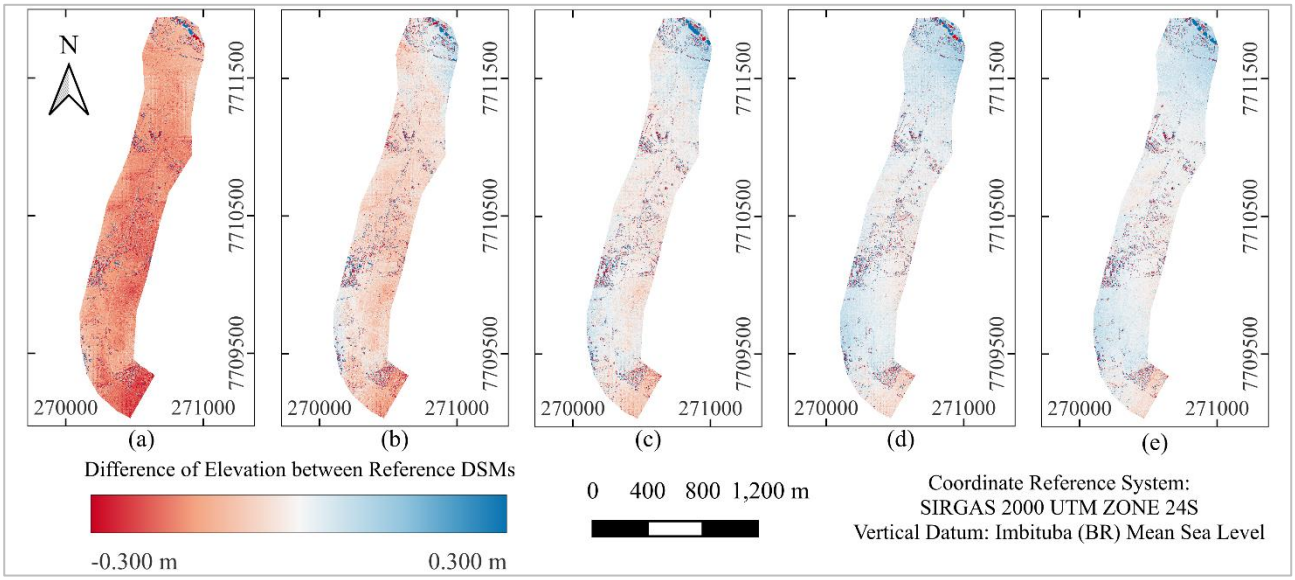

Figure 3. Difference of Elevation (DoD) between estimated and reference DSMs: (a-e) DoD between estimated DSMs (OTJCalib, GNSS-AAT_1 to GNSS-AAT_4) and Ref_DSM.

When a sub-block of oblique images (pitch = 18°) was added for both camera calibration (OSCalib_2) and spatial data acquisition (GNSS-AAT_2), the elevation residuals showed better spatial distribution on the DoD between GNSS-AAT_2_DSM and Ref_DSM (Figure 3c). Although the north edge still exhibited positive residuals and the south edge more negative residuals, the overall corridor area displayed a well-distributed pattern close to zero, indicating no significant spatial bias.

Conversely, incorporating a sub-block of oblique images with a 45° pitch (GNSS-AAT_3) revealed positive elevation residuals across most of the DoD between GNSS-AAT_3_DSM and Ref_DSM (Figure 3d), except in the southern edge of the block. Similar results were observed in the experiment that included two oblique sub-blocks (18° and 45° pitch), as seen in the DoD between GNSS-AAT_4_DSM and Ref_DSM (Figure 3e). Both the GNSS-AAT_3 and GNSS-AAT_4 experiments showed a slightly positive bias across the corridor, while still maintaining some areas with negative residuals.

Taking a closer look at the elevation residuals displayed in Figure 3, the gradient error range (-0.3 m to 0.3 m) was selected, representing approximately 99% of the data, to highlight the overall error distribution. Residuals outside this range (>0.3 m and <−0.3 m) were represented with darker red and blue. This ensured that significantly high elevation residuals from outliers didn't disproportionately affect the gradient colors.

In the DoD outcomes (Figure 3), significantly high elevation residuals (reaching up to 30 m) were originated from points, in the dense cloud, located at the edges of features such as buildings and high/dense vegetation. Even after the *Point Cloud Confidence* filter was applied, remaining low-confidence points on object borders caused high variations in elevation values across different experiments, leading to substantial residual values when comparing the generated DSMs to the Ref_DSM. Although these noises were present, residuals greater than 1 m represented a very low percentage (approximately 1.6%) of the overall data.

Finally, to provide a quantitative investigation of DSMs' precisions, the median and Interquartile range (IQR) were calculated for all DoD results. Figure 4 displays the boxplot for DoD from DSMs. The outlier thresholds were established by the lower limit of '1st quartile -1.5*IQR' and the upper limit of '3rd quartile + 1.5*IQR'.

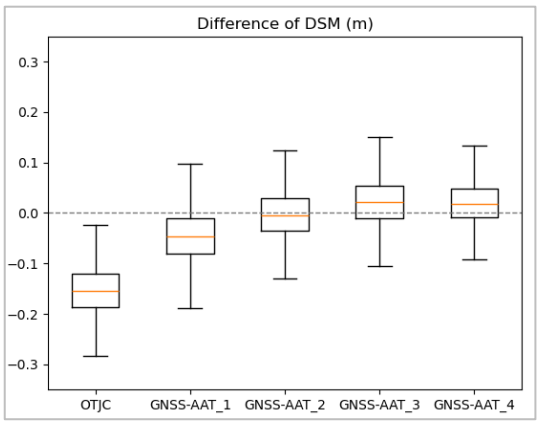

Figure 4. Boxplot chart of DSMs' residuals.

Based on the boxplot results, the OTJCalib experiment showed the highest bias in DSMs, with a median of -0.153 m. As confirmed by the 2D visualization of DoD from DSM (Figure 3a), the OTJCalib_DSM seems to be entirely dislocated below the reference surface (Ref_DSM) by showing only shades of red (negative elevation residuals). When analyzing the GNSS-AAT_1_DSM residuals, the median value shows a negative value of -0.047 m, but about 25% of the residuals were positive, appearing as light blue residuals in Figure 3b. These results are particularly interesting given that GNSS-AAT_1 utilizes IOPs from OSCalib_1, which was performed with a sub-block of 40 vertical images located in the center-south region of the corridor block.

This contribution has been peer-reviewed. The double-blind peer-review was conducted on the basis of the full paper.
https://doi.org/10.5194/isprs-annals-X-3-W4-2025-293-2026 | © Author(s) 2026. CC BY 4.0 License.

In that sense, the same dataset (279 vertical images) was used for both analyzed experiments (OTJCalib and GNSS-AAT_1), and their IOPs were also estimated using only vertical images (a full block for OTJCalib and a sub-block for GNSS-AAT_1). However, the vertical accuracy (in RMSE Z of checkpoints discrepancies) and the overall vertical precision (compared to the Ref_Calib) were significantly improved by performing an on-situ pre-calibration. In other words, using a sub-block of images for on-site pre-calibration, even with only vertical images and the same dataset for spatial data acquisition, showed about a 70% improvement in accuracy and precision for the corridor's elevation.

For the experiments that included sub-blocks of oblique images, when using the sub-block with an 18° pitch, the median value was -0.004 m for the residuals of DoD from GNSS-AAT_3_DSM. Figure 4 also exhibits a symmetrical distribution of residuals around the zero axis, closely resembling a normal distribution. These residuals and their spatial distribution (Figure 3c) indicate that the GNSS-AAT_2 experiment, by adding one sub-block of 19 oblique images with an 18° pitch (representing only 7% of the corridor's vertical block of 279 images), could achieve statistical results for elevation values surprisingly close to the Ref_Calib experiment, which includes 17GCPs in the center line of the block. In other words, the GNSS-AAT_2 experiment, without GCPs but only incorporating a small subset of oblique images, generated an elevation surface (DSM) equivalent to that from the experiment with a dense distribution of GCPs (Ref_DSM).

In contrast, adding a sub-block of oblique images with a 45° pitch resulted in a slight positive bias in the DSMs residuals, with a median of 0.021 m on the GNSS-AAT_3_DSM. Similar results were achieved when both oblique sub-blocks were added in the GNSS-AAT_4 experiment, which showed a median of 0.018 m.

Overall, the outcomes show that all four GNSS-AAT experiments with on-site pre-calibration provided significantly better precision than the on-the-job calibration, for DSM surfaces. Even when using the exact same vertical dataset, performing on-site pre-calibration (GNSS-AAT_1) successfully improved the elevation precision from the OTJCalib experiment, though a negative bias on the elevation surfaces still persisted. Ultimately, the best precision result was achieved with GNSS-AAT_2 when an 18° pitch sub-block was incorporated, yielding results similar to the DSM generated by the reference experiment with GCPs.

4. Limitations and Future Work

This study achieved promising outcomes in improving the accuracy and precision of vertical spatial data acquired for corridors by UAS photogrammetry without the need for Ground Control Points (GCPs). A remaining limitation is that the proposed approach was tested in a single study site. Therefore, to improve the robustness and generalizability of the findings it is advised to apply it in other corridor areas with different terrain features and topographies, such as coastal regions, riverbanks, and glacial areas. Moreover, it is also recommended to replicate the methodology with different equipment, including various cameras, UAV platforms, and SfM-MVS software.

5. Conclusions

It is well-known that integrating oblique imagery enhances Interior Orientation Parameter (IOP) estimation and improves overall spatial data acquisition accuracy by UAS-photogrammetry. However, existing studies have not sufficiently explored feasible methods for incorporating oblique images into corridor blocks for camera calibration, particularly how this impacts subsequent 3D products such as Digital Surface Models (DSMs). This study addressed this gap, contributing to UAS photogrammetry for corridor mapping by proposing an approach with on-site pre-calibrations using a sub-block of images and demonstrating significant improvements in vertical accuracy and 3D model precision without Ground Control Points (GCPs).

To that end, five camera calibration experiments were conducted: one on-the-job calibration (OTJCalib) and four on-site pre-calibrations (OSCalib_1 to OSCalib_4) using various sub-block configurations, including multi-height oblique images. The IOPs estimated with pre-calibrations were then applied in corresponding GNSS-Assisted Aerial Triangulation (GNSS-AAT) experiments to generate tie points, dense point clouds, and DSMs. An important result from parameter correlation analysis revealed that including oblique images in sub-block calibrations substantially reduced the high correlation between focal length and Z object-space coordinates (from 99% to less than 20%). This led to improved focal length estimation and reduced vertical systematic errors in DSMs. Conversely, correlations impacting horizontal accuracy remained unchanged across all tested calibration strategies.

The outcomes demonstrate that on-site sub-block calibration significantly improved the precision of generated DSMs. Analysis of the Difference of DSM (DoD) for the OTJCalib revealed a clear negative bias in the elevation residuals, indicating a consistent vertical offset when no GCPs and oblique images were used. In contrast, GNSS-AAT experiments utilizing on-site pre-calibrations with sub-blocks yielded DSMs with significantly higher precision. Particularly, GNSS-AAT_2 (including an 18° pitch oblique sub-block) showed elevation residuals close to zero, yielding results similar to the DSM generated by the reference experiment with a dense distribution of GCPs. This indicates that a small, strategically acquired set of oblique images for on-site pre-calibration can effectively reduce bias on DSMs, even without GCPs. Although conducted in a singular test area, this approach significantly enhanced the accuracy and precision of geospatial data extraction in UAS photogrammetry for corridors, reducing the requirement for dense GCP distributions.

Acknowledgments

The authors would like to thank the Brazilian governmental agencies CNPq (The National Council for Scientific and Technological Development) for the PhD grant and CAPES (The Coordinating Agency for Advanced Training of High-Level Personnel) for the Institutional Internationalization Program (PrInt) grant, which funded this study.

References

Ait-Lamallam, S., Lamrani, R., Mastari, W., Kechna, M., 2025. Effective Strategies for Mitigating the "Bowl" Effect and Optimising Accuracy: A Case Study of UAV Photogrammetry in Corridor Projects. *Drones*, 9(6), 387.

Amorim, N., Mitishita, E., 2024. Avaliação da precisão da técnica Structure from Motion aplicada ao Mapeamento Fotogramétrico de Corredores. LUMEN ET VIRTUS, 15(39), 2041-2056.

Andaru, R., Rau, J. Y., Chuang, L. Z. H., Jen, C. H, 2022. Multitemporal UAV photogrammetry for sandbank morphological change analysis: evaluations of camera calibration methods, co-registration strategies, and the reconstructed DSMs. *IEEE Journal of Selected Topics in Applied Earth Observations and Remote Sensing*, *15*, 5924-5942.

Brock, J., Schratz, P., Petschko, H., Muenchow, J., Micu, M., Brenning, A, 2020. The performance of landslide susceptibility models critically depends on the quality of digital elevation models. *Geomatics, Natural Hazards and Risk*, 11(1), 1075-1092.

Carbonneau, P. E., & Dietrich, J. T., 2017. Cost-effective non-metric photogrammetry from consumer-grade sUAS: implications for direct georeferencing of structure from motion photogrammetry. *Earth surface processes and landforms*, 42(3), 473-486.

Chiabrando, F., Giulio Tonolo, F., & Lingua, A., 2019. Uav direct georeferencing approach in an emergency mapping context. The 2016 central Italy earthquake case study. *The International Archives of the Photogrammetry, Remote Sensing and Spatial Information Sciences*, 42, 247-253.

Clédat, E., Cucci, D. A., Skaloud, J., 2020. Camera calibration models and methods for corridor mapping with UAVS. *ISPRS Annals of the Photogrammetry, Remote Sensing and Spatial Information Sciences*, *1*, 231-238.

Costa, F. A., Mitishita, E. A., Martins, M., 2018. The influence of sub-block position on performing integrated sensor orientation using in situ camera calibration and lidar control points. *Remote Sensing*, *10*(2), 260.

Darji, K., Patel, D., Dubey, A.K., Gupta, P.K., Singh, R.P, 2024. UAV (Drone) for Preparation of High-Resolution DEM/DTM—A Case Application of Post Flood Assessment of Dhanera City, Rel River Catchment. In: Timbadiya, P.V., Patel, P.L., Singh, V.P., Manekar, V.L. (eds) *Flood Forecasting and Hydraulic Structures. HYDRO 2021*. Lecture Notes in Civil Engineering, vol 340. Springer, Singapore.

Deliry, S. I., Avdan, U., 2021. Accuracy of unmanned aerial systems photogrammetry and structure from motion in surveying and mapping: a review. *Journal of the Indian Society of Remote Sensing*, *49*(8), 1997-2017.

Ferrer-González, E., Agüera-Vega, F., Carvajal-Ramírez, F., Martínez-Carricondo, P., 2020. UAV photogrammetry accuracy assessment for corridor mapping based on the number and distribution of ground control points. *Remote sensing*, *12*(15), 2447.

Forlani, G., Dall'Asta, E., Diotri, F., Morra di Cella, U., Roncella, R., Santise, M., 2018. Quality assessment of DSMs produced from UAV flights georeferenced with on-board RTK positioning. *Remote sensing*, *10*(2), 311.

Guth, P. L., Van Niekerk, A., Grohmann, C. H., Muller, J. P., Hawker, L., Florinsky, I. V., ... & Strobl, P. (2021). Digital elevation models: Terminology and definitions. *Remote Sensing*, 13(18), 3581.

Hashimoto, A., Inokoshi, S., Chiu, C. W., Onda, Y., Gomi, T., Uchiyama, Y, 2025. Estimating characteristics of planted forests' relative yield index using low pulse density LiDAR and satellite remote sensing. *International Journal of Applied Earth Observation and Geoinformation*, 139, 104558.

Huang, D., Tang, Y., Qin, R, 2022. An evaluation of planetscope images for 3d reconstruction and change detection–experimental validations with case studies. *GIScience & Remote Sensing*, 59(1), 744-761.

Kraus, K., 2007. Photogrammetry: geometry from images and laser scans. Walter de Gruyter: Berlin, Germany. 2nd English Ed., Translated by: Harley, I., Kyle, S.

La Salandra, M., Colacicco, R., Dellino, P., Capolongo, D., 2023. An effective approach for automatic river features extraction using high-resolution UAV imagery. *Drones*, *7*(2), 70.

Lenda, G., Borowiec, N., Marmol, U, 2023. Study of the Precise Determination of Pipeline Geometries Using UAV Scanning Compared to Terrestrial Scanning, Aerial Scanning and UAV Photogrammetry. *Sensors*, 23(19), 8257.

Liu, X., Lian, X., Yang, W., Wang, F., Han, Y., Zhang, Y., 2022. Accuracy assessment of a UAV direct georeferencing method and impact of the configuration of ground control points. *Drones*, *6*(2), 30.

Luhmann, T., Robson, S., Kyle, S., Harley, I., 2006. *Close range photogrammetry*. Caithness, UK: Wiley Whittles Publishing.

Meinen, B. U., Robinson, D. T., 2020. Streambank topography: An accuracy assessment of UAV-based and traditional 3D reconstructions. *International Journal of Remote Sensing*, *41*(1), 1-18.

Mitishita, E., Barrios, R., Centeno, J., 2014. The influence of the in situ camera calibration for direct georeferencing of aerial imagery. *The International Archives of the Photogrammetry, Remote Sensing and Spatial Information Sciences*, *40*, 273-278.

Pessoa, G., Carrilho, A., Miyoshi, G., Amorim, A., Galo, M., 2020. Assessment of UAV-based digital surface model and the effects of quantity and distribution of ground control points. International Journal of Remote Sensing, 42(1), 65–83.

Pilartes-Congo, J. A., Starek, M. J., Pashaei, M., Berryhill, J., 2024. Examination of UAS-SfM and UAS-Lidar for Survey Repeatability of Roadway Corridors. In *IGARSS 2024-2024 IEEE International Geoscience and Remote Sensing Symposium* (pp. 6605-6608). IEEE.

Pinton, D., Canestrelli, A., Moon, R., Wilkinson, B, 2022. Estimating ground elevation in coastal dunes from high-resolution UAV-LIDAR Point Clouds and Photogrammetry. *Remote Sensing*, 15(1), 226.

Pitombeira, K., Mitishita, E., 2023. Influence of On-Site Camera Calibration with Sub-Block of Images on the Accuracy of Spatial Data Obtained by PPK-Based UAS Photogrammetry. *Remote Sensing*, *15*(12), 3126.

Pitombeira, K., Mitishita, E., Toth, C., de Abreu, M. (2025). On-site camera calibration with sub-block of images for UAS Photogrammetry corridor mapping with on-board GNSS-RTK. ISPRS Annals of the Photogrammetry, Remote Sensing and Spatial Information Sciences, 657-664.

Remondino, F., Fraser, C., 2006. Digital camera calibration methods: considerations and comparisons. *International Archives of the Photogrammetry, Remote Sensing and Spatial Information Sciences*, *36*(5), 266-272.

Sanz-Ablanedo, E., Chandler, J. H., Ballesteros-Pérez, P., Rodríguez-Pérez, J. R, 2020. Reducing systematic dome errors in digital elevation models through better UAV flight design. *Earth Surface Processes and Landforms*, 45(9), 2134-2147.

Senkal, E., Kaplan, G., Avdan, U, 2021. Accuracy assessment of digital surface models from unmanned aerial vehicles' imagery on archaeological sites. *International Journal of Engineering and Geosciences*, 6(2), 81-89.

Skondras, A., Karachaliou, E., Tavantzis, I., Tokas, N., Valari, E., Skalidi, I., ... & Stylianidis, E, 2022. UAV Mapping and 3D Modeling as a Tool for Promotion and Management of the Urban Space. *Drones*, 6(5), 115.

Smith, M. W., Carrivick, J. L., Quincey, D. J., 2016. Structure from motion photogrammetry in physical geography. *Progress in physical geography*, *40*(2), 247-275.

Sobura, S, 2022. Calibration of the low-cost UAV camera on a spatial test field. *Geodesy and Cartography*, 48(3), 134-143.

Štroner, M., Urban, R., Křemen, T., Braun, J, 2023. UAV DTM acquisition in a forested area–comparison of low-cost photogrammetry (DJI Zenmuse P1) and LiDAR solutions (DJI Zenmuse L1). *European Journal of Remote Sensing*, 56(1), 2179942.

Wackrow, R., Chandler, J. H, 2008. A convergent image configuration for DEM extraction that minimises the systematic effects caused by an inaccurate lens model. *The Photogrammetric Record*, 23(121), 6-18.

Zhang, H., Aldana-Jague, E., Clapuyt, F., Wilken, F., Vanacker, V., Van Oost, K., 2019. Evaluating the potential of post-processing kinematic (PPK) georeferencing for UAV-based structure-from-motion (SfM) photogrammetry and surface change detection. *Earth Surface Dynamics*, 7(3), 807-827.